

Vortices in Thin, Compressible, Unmagnetized Disks

Bryan M. Johnson and Charles F. Gammie

*Center for Theoretical Astrophysics, University of Illinois at Urbana-Champaign, 1110
West Green St., Urbana, IL 61801*

ABSTRACT

We consider the formation and evolution of vortices in a hydrodynamic shearing-sheet model. The evolution is done numerically using a version of the ZEUS code. Consistent with earlier results, an injected vorticity field evolves into a set of long-lived vortices each of which has radial extent comparable to the local scale height. But we also find that the resulting velocity field has positive shear stress $\langle \Sigma \delta v_r \delta v_\phi \rangle$. This effect appears only at high resolution. The transport, which decays with time as $t^{-1/2}$, arises primarily because the vortices drive compressive motions. This result suggests a possible mechanism for angular momentum transport in low-ionization disks, with two important caveats: a mechanism must be found to inject vorticity into the disk, and the vortices must not decay rapidly due to three-dimensional instabilities.

Subject headings: accretion, accretion disks, solar system: formation, galaxies: nuclei

1. Introduction

Astrophysical disks are common because the specific angular momentum of the matter inside them is well-conserved. They evolve because angular momentum conservation is weakly compromised, either because of diffusion of angular momentum within the disk or because of direct application of external torques.

In astrophysical disks composed of a well-ionized plasma it is likely that some, perhaps most, of the evolution is driven by diffusion of angular momentum within the disk. This view is certainly consistent with observations of steadily accreting cataclysmic variable systems like UX Ursae Majoris (Baptista et al. 1998; Baptista 2004), whose radial surface-brightness profile is consistent with steady accretion-flow models in which the bulk of the accretion energy is dissipated within the disk.

Angular momentum diffusion in well-ionized disks is likely driven by magnetohydrodynamic (MHD) turbulence. Analytic analyses, numerical experiments, and laboratory evidence strongly suggest that well-coupled plasmas in differentially-rotating flows are subject to the magnetorotational instability (MRI; Balbus & Hawley 1991, 1998; Balbus 2003). But MHD turbulence is initiated by the MRI only so long as the plasma is sufficiently ionized to couple to the magnetic field (Kunz & Balbus 2004; Desch 2004). In disks around young stars, cataclysmic-variable and X-ray binary disks in quiescence, and possibly the outer parts of AGN disks, the plasma may be too neutral to support magnetic activity (Gammie & Menou 1998; Menou 2000; Stone, Gammie, Balbus, & Hawley 2000; Menou & Quataert 2001; Fromang et al. 2002). This motivates interest in non-MHD angular momentum transport mechanisms.

Within the last few years, a body of work has been developed suggesting that vortices can be generated as a result of global hydrodynamic instability (Hawley 1987; Blaes & Hawley 1988; Hawley 1990; Lovelace, Li, Colgate, & Nelson 1999; Li, Finn, Lovelace, & Colgate 2000) or local hydrodynamic instability (Klahr & Bodenheimer 2003), that vortices in disks may be long-lived (Godon & Livio 1999, 2000; Umurhan & Regev 2004; Barranco & Marcus 2005), and that these vortices may be related to an outward flux of angular momentum (Li, Colgate, Wendroff, & Liska 2001; Barranco & Marcus 2005). If these claims can be verified then the consequences for low-ionization disks would be profound.

Here we investigate the evolution of a disk that is given a large initial vortical velocity perturbation. Our study is done in the context of a (two-dimensional) shearing-sheet model, which permits us to resolve the dynamics to a degree that is not currently possible in a global disk model. Our model is also fully compressible, unlike previous work using a local model (Umurhan & Regev 2004; Barranco & Marcus 2005). The former assume incompressible flow and the latter use the anelastic approximation (e.g., Gough 1969), which filters out the high-frequency acoustic waves. We will show that compressibility and acoustic waves play an essential part in the angular momentum transport.

Our paper is organized as follows. In §2 we describe the model. In §3 we describe the evolution of a fiducial, high-resolution model. In §4 we investigate the dependence of the results on model parameters. And in §5 we describe implications, with an emphasis on key open questions: are the vortices destroyed by three-dimensional instabilities?; and do mechanisms exist that can inject vorticity into the disk?

2. Model

The shearing-sheet model is obtained via a rigorous expansion of the two-dimensional hydrodynamic equations of motion to lowest order in H/R , where $H = c_s/\Omega$ is the disk scale height (c_s is the isothermal sound speed and Ω is the local rotation frequency) and R is the local radius. See Narayan et al. (1987) for a description. Adopting a local Cartesian coordinate system where the x axis is oriented parallel to the radius vector and the y axis points forward in azimuth, the equations of motion become

$$\frac{d\Sigma}{dt} + \Sigma \nabla \cdot \mathbf{v} = 0, \quad (1)$$

$$\frac{d\mathbf{v}}{dt} + \frac{\nabla P}{\Sigma} + 2\Omega \times \mathbf{v} - 2q\Omega^2 x \hat{\mathbf{x}} = 0, \quad (2)$$

where Σ and P are the two-dimensional density and pressure, \mathbf{v} is the fluid velocity and d/dt is the Lagrangian derivative. The third and fourth terms in equation (2) represent the Coriolis and centrifugal forces in the local model expansion, where $q = -(1/2) d \ln \Omega^2 / d \ln r$ is the shear parameter. We will assume throughout that $q = 3/2$, corresponding to a Keplerian shear profile. We close the above equations with an isothermal equation of state

$$P = c_s^2 \Sigma, \quad (3)$$

where c_s is constant in time and space.

Equations (1) through (3) can be combined to show that the vertical component of potential vorticity

$$\xi \equiv \frac{(\nabla \times \mathbf{v} + 2\Omega) \cdot \hat{\mathbf{z}}}{\Sigma} \quad (4)$$

is a constant of the motion; i.e., the potential vorticity of fluid elements in two dimensions is conserved.

An equilibrium solution to the equations of motion is

$$\Sigma = \Sigma_0 = \text{const.} \quad (5)$$

$$P = c_s^2 \Sigma_0 = \text{const.} \quad (6)$$

$$v_x = 0 \quad (7)$$

$$v_y = -q\Omega x \quad (8)$$

Thus the differential rotation of the disk makes an appearance in the form of a linear shear.

We integrate the above equations using a version of the ZEUS code (Stone & Norman 1992). ZEUS is a time-explicit, operator-split scheme on a staggered mesh. It uses artificial

viscosity to capture shocks. Our computational domain is a rectangle of size $L_x \times L_y$ containing $N_x \times N_y$ grid cells. The numerical resolution is therefore $\Delta x \times \Delta y = L_x/N_x \times L_y/N_y$.

Our code differs from the standard ZEUS algorithm in two respects. First, we have implemented a version of the shearing-box boundary conditions. The model is then periodic in the y direction; the x boundaries are initially joined in a periodic fashion, but they are allowed to shear with respect to each other, becoming periodic again when $t = nL_y/(q\Omega L_x)$, $n = 1, 2, \dots$. A detailed description of the boundary conditions is given in Hawley, Gammie, & Balbus (1995).

Second, we treat advection by the mean flow $\mathbf{v}_0 = -q\Omega x \hat{\mathbf{y}}$ separately from advection by the perturbed flow $\delta\mathbf{v} \equiv \mathbf{v} - \mathbf{v}_0$. Mean-flow advection can be done by interpolation, using the algorithm described in Gammie (2001), which is similar to the FARGO scheme (Masset 2000). This has the advantage that the timestep is not limited by the mean flow velocity (it is $|\delta\mathbf{v}|$ rather than $|\mathbf{v}|$ that enters the Courant condition). This permits the use of a timestep that is larger than the usual timestep by $\sim L_x/H$ if $L_x \gg H$. The shear-interpolation scheme also makes the algorithm more nearly translation-invariant in the $x - y$ plane, thereby more nearly embodying an important symmetry of the underlying equations.

2.1. Initial Conditions

Without a specific model for the process that is injecting the vorticity, it is difficult to settle on a particular set of initial conditions, or to know how these initial conditions ought to vary when the size of the box is allowed to vary. Our choice of initial conditions is therefore somewhat arbitrary. We use a set of initial (incompressive) velocity perturbations drawn from a Gaussian random field. The amplitude of the perturbations is characterized by $\sigma = \langle |\delta\mathbf{v}/c_s|^2 \rangle^{1/2}$. The power spectrum is $|\delta\mathbf{v}|^2 \sim k^{-8/3}$, corresponding to the energy spectrum ($E_k \sim k^{-5/3}$) of a two-dimensional Kolmogorov inverse turbulent cascade, with cutoffs at $k_{min} = (1/2)(2\pi/H)$ and $k_{max} = 32k_{min}$ ¹. The surface density is not perturbed. These initial conditions correspond to a set of purely vortical perturbations. The parameters for our fiducial run are $L_x = L_y = 4H$ and $\sigma = 0.4$.

¹We have compared our fiducial run to runs with a different range in k , corresponding to vorticity injection either at scales $\sim H$ or scales $\sim 0.1H$. The results are qualitatively the same.

2.2. Code Verification

Although our basic algorithm has already been tested (see Gammie 2001), we test the current version of our code by making a comparison with linear theory. Due to the underlying shear, small-amplitude perturbations in the shearing sheet are naturally decomposed in terms of shearing waves or *shwaves* (see Johnson & Gammie 2005 and references therein), Fourier components in the “co-shearing” frame. These have time-dependent wavenumber $\mathbf{k}(t) = k_x(t)\hat{\mathbf{x}} + k_y\hat{\mathbf{y}}$, where $k_x(t) = k_{x0} + q\Omega k_y t$ and k_{x0} and k_y are constant. The evolution of a single Fourier component can be calculated by integrating an ordinary differential equation for the amplitude of the shwave. For purely vortical (nonzero *potential* vorticity) or non-vortical perturbations, the evolution can be obtained analytically. The explicit expression for the amplitude of a vortical (incompressive) shwave is

$$\delta v_{xi} = \delta v_{x0} \frac{k_0^2}{k^2} = \delta v_{x0} \frac{1 + \tau_0^2}{1 + \tau^2}, \quad (9)$$

where $k^2 = k_x^2 + k_y^2$, $\tau = q\Omega t + k_{x0}/k_y$ and a subscript 0 on a quantity indicates its value at $t = 0$.² The amplitude of a non-vortical (compressive) shwave satisfies the differential equation

$$\frac{d^2 \delta v_{yc}}{dt^2} + (c_s^2 k^2 + \Omega^2) \delta v_{yc} = 0, \quad (10)$$

the solutions of which are parabolic cylinder functions. See Johnson & Gammie (2005) for further details on the shwave solutions.

Figure 1 compares the numerical evolution of both vortical and compressive shwave amplitudes with their analytic solutions. The initial shwave vector (k_{x0}, k_y) is $(-16\pi/L_x, 4\pi/L_y)$ for the vortical shwave and $(-8\pi/L_x, 2\pi/L_y)$ for the compressive shwave. The other model parameters are the same as those in the fiducial run, except that $L = 0.5H$ for the vortical-shwave evolution since $k_y H \gg 1$ is required to prevent mixing between vortical and non-vortical shwaves near $\tau = 0$. The shwaves are well resolved until the radial wavelength $\lambda_x = 4 \times \Delta x$, and the code is capable of tracking both potential-vorticity and compressive perturbations with high accuracy.

3. Results

The evolution of the potential vorticity in our fiducial run is shown in Figure 2. The snapshots are shown in lexicographic order beginning with the initial conditions, which have

²This solution is valid at all times only for short-wavelength vortical perturbations ($kH \gg 1$).

equal positive and negative $\delta\xi$.

One of the most remarkable features of the fiducial run evolution is the appearance of comparatively-stable, long-lived vortices. These vortices have negative $\delta\xi$ and are therefore dark in Figure 2. Similar vortices have been seen by Godon & Livio (1999, 2000), Li, Colgate, Wendroff, & Liska (2001) and Umurhan & Regev (2004). Cross sections of one of the vortices at the end of the run are shown in Figure 3. In our models the vortices are not associated with easily identifiable features in the surface density, since the perturbed vorticity is not large enough to require, through the equilibrium condition, an order unity increase in the local pressure.

While the vortices are long-lived, they do decay. Figure 4 shows the evolution of the perturbed (noncircular) kinetic energy

$$E_K \equiv \frac{1}{2} \Sigma (\delta v_x^2 + \delta v_y^2) \quad (11)$$

in the fiducial run. Evidently the kinetic energy decays approximately as $t^{-1/2}$ (which is remarkable in that, if the vortices would correspond to features in *luminosity* that decay as $t^{-1/2}$, they could produce flicker noise; see Press 1978). Runs with half and twice the resolution decay in the same fashion, but if the resolution is reduced to 64^2 the kinetic energy decays exponentially. Resolution of at least 128 zones per scale height appears to be required.

What is even more remarkable is that the vortices are associated with an outward angular momentum flux, due to the driving of compressive motions by the vortices. Figure 5 shows the evolution of the dimensionless angular momentum flux

$$\alpha \equiv \frac{1}{L_x L_y \Sigma_0 c_s^2} \int \Sigma \delta v_x \delta v_y dx dy \quad (12)$$

for models with a variety of resolutions. The data has been boxcar smoothed over an interval $\Delta t = 10\Omega^{-1}$ to make the plot readable. Again, a resolution of at least 512^2 appears to be required for a converged measurement of the shear stress. For the most highly resolved models α evolves like the kinetic energy, $\propto t^{-1/2}$.

Compressibility is crucial for development of the angular momentum flux. We have demonstrated this in two ways. First, we have taken the fiducial run and decomposed the velocity field into a compressive and an incompressive part (i.e., into potential and solenoidal pieces in Fourier space) and measured the stress associated with each. For a set of snapshots taken from the last half of the fiducial run, the average total $\alpha = 0.0036$; the incompressive component is $\alpha_i = -0.0006$; the compressive component is $\alpha_c = 0.0032$. The remaining alpha $\alpha_x = 0.00099$ is in cross-correlations between the incompressive and

compressive pieces of the velocity field. As argued in Balbus (2000) and Balbus (2003), both incompressive trailing shwaves and incompressible turbulence transport angular momentum inward, whereas trailing compressive disturbances transport angular momentum outward. Our negative (positive) value for α_i (α_c) is consistent with this.

Second, we have reduced the size of the model and reduced the amplitude of the initial perturbation so that it scales with the shear velocity at the edge of the model (constant “intensity” of the turbulence, in Umurhan and Regev’s parlance). Thus the Mach number of the turbulence is reduced in proportion to the size of the box. We have compared four models, with $L = (4, 2, 1, 0.5)H$ and $\sigma = (0.8, 0.4, 0.2, 0.1)c_s$. We would expect the lower Mach number models to have smaller-amplitude compressive velocity fields and therefore, consistent with the above results, smaller angular momentum flux α . Averaging over the second half of the simulation, we find $\alpha = (0.0031, 0.0018, 7.2 \times 10^{-5}, -9.5 \times 10^{-7})$.

An additional confirmation of our overall picture can be seen in Figure 6, in which we show a snapshot of the velocity divergence superimposed on the potential vorticity for a medium-resolution (256^2) version of the fiducial run.³ The position of the shocks with respect to the vortices in this figure is consistent with our interpretation that the former are generated by the latter.

The smallest of our simulations ($L = 0.5H$) is nearly incompressible, but we continue to observe $t^{-1/2}$ decay (least squares fit power law is -0.49) at late times. The reason that we see decay while Umurhan & Regev (2004) do not may be that: (1) the remaining compressibility in our model causes added dissipation; (2) the numerical dissipation in our code is larger than that of Umurhan & Regev (2004); (3) the code used by Umurhan & Regev (2004) could somehow be aliasing power from trailing shwaves to leading shwaves (although they do explicitly discuss, and dismiss, this possibility).

To highlight the dangers of aliasing for our finite-difference code, in Figure 7 we show the evolution of a vortical shwave amplitude at low resolution (64^2), in units of τ . We use the same parameters as those in our linear-theory test (Figure 1), for which the initial shwave vector corresponds to $\tau_0 = -4$. The initially-leading shwave swings into a trailing shwave, the radial wavelength is eventually lost near the grid scale, and due to aliasing the code picks up the evolution of the shwave again as a leading shwave. Repeating this test at higher resolutions indicates that successive swings from leading to trailing occur at an interval of $\tau = N_x/n_y$, where $n_y = 2$ is the azimuthal wavenumber of the shwave. This is equivalent to $k_x(t) = 2\pi/\Delta x$. The decay of the successive linear solutions with time is due to numerical

³At higher resolutions, shocks are generated earlier in the simulation from smaller vortices, and it is more difficult to see the effect we are describing due to the random nature of the vortices at this early stage.

diffusion.

Figure 7 suggests that it is easier to inject power into the simulation due to aliasing rather than to remove power due to numerical diffusion. We do not believe, however, that aliasing is affecting our high-resolution results. In addition, if we assume that the flow in our simulations can be modeled as two-dimensional Kolmogorov turbulence, then $\delta v_{rms} \sim \lambda^{1/3}$, where δv_{rms} is the rms velocity variation across a scale λ . The velocity due to the mean shear at these scales is $\delta v_{shear} \sim q\Omega\lambda$, and $\delta v_{rms}/\delta v_{shear} \sim \lambda^{-2/3}$. The velocities at the smallest scales are thus dominated by turbulence rather than by the mean shear. This conclusion is supported by the convergence of our numerical results at high resolution.

Our model contains two additional numerical parameters: the size L and the initial turbulence amplitude σ . Figure 8 shows the evolution of α for several values of σ . Evidently for small enough values of σ the α amplitude is reduced, but for near-sonic initial Mach numbers the α amplitude saturates (or at least the dependence on σ is greatly weakened). Figure 9 shows the evolution for several values of L but the same initial σ and the identical initial power spectrum. For large enough L the shear stress appears to be independent of L .

Finally, we have studied the autocorrelation function of the potential vorticity as a means of characterizing structure inside the flow. Figure 10 shows the autocorrelation function measured in the fiducial model and in an otherwise identical model with $L = 8H$. Evidently the potential vorticity is correlated over about one-half a scale height in radius, independent of the size of the model. This supports the idea that compressive effects limit the size of the vortices, since the shear flow becomes supersonic across a vortex of size $\sim H$ (Barge & Sommeria 1995; Li, Colgate, Wendroff, & Liska 2001).

4. Conclusion

The presence of long-lived vortices in weakly-ionized disks may be an integral part of the angular momentum transport mechanism in these systems. The key result we have shown here is that compressibility of the flow is an extremely important factor in providing a significant, positively-correlated average shear stress with its associated outward transport of angular momentum. Previous results using a local model have assumed incompressible flow and either report no angular momentum transport (Umurhan & Regev 2004) or report a value ($\alpha \sim 10^{-5}$, Barranco & Marcus 2005) that is two orders of magnitude lower than what we find when we include the effects of compressibility. Global simulations (Godon & Livio 1999, 2000; Li, Colgate, Wendroff, & Liska 2001) have a difficult time accessing the high resolution that we have shown is required for a significant shear stress due to compressibility.

Our work leaves open the key question of what happens in three dimensions. Our vortices, which have radial and azimuthal extent $\lesssim H$, are inherently three-dimensional. Three-dimensional vortices are susceptible to the elliptical instability (Kerswell 2002) and are likely to be destroyed on a dynamical timescale. The fact that vortices persist in our two-dimensional simulations and not in the local (three-dimensional) shearing-box calculations of Balbus et al. (1996) is likely due to dimensionality. The recent numerical results of Barranco & Marcus (2005) indicate that vortices near the disk midplane are quickly destroyed, whereas vortices survive if they are a couple of scale heights away from the midplane. Strong vertical stratification away from the midplane may enforce two-dimensional flow and allow the vortices that we consider here to survive.

The initial conditions in Barranco & Marcus (2005) are analytic solutions for two-dimensional vortices that are stacked into a three-dimensional column. The stable, off-midplane vortices apparently arise due to the breaking of internal gravity waves generated by the midplane vortices before they become unstable. There is also an unidentified instability that breaks a single off-midplane vortex into several vortices. These simulations leave open the question of whether stable off-midplane vortices can be generated from a random set of initial vorticity perturbations rather than the special vortex solutions that are imposed.

Our work also leaves open the key question of what generates the initial vorticity. One possibility is that material builds up at particular radii in the disk, resulting in a global instability (e.g. Papaloizou & Pringle 1984, 1985) and a breakdown of the flow into vortices (Li, Colgate, Wendroff, & Liska 2001). A second possibility for vortex generation in variable systems is that the MHD turbulence, which likely operates during an outburst but decays as the disk cools (Gammie & Menou 1998), leaves behind some residual vorticity. The viability of such a mechanism could be tested with non-ideal MHD simulations such as those of Fleming & Stone (2003) and Sano & Stone (2003). A third possibility is that differential illumination of the disk somehow produces vorticity. Since the temperature of most circumstellar disks is controlled by stellar illumination, small variations in illumination could produce hot and cold spots in the disk that interact to produce vortices. A fourth possibility is the generation of vorticity via baroclinic instability, which is likely to operate in disks whose vertical stratification is close to adiabatic (Knobloch & Spruit 1986). The nonlinear outcome of this instability in planetary atmospheres is the formation of vortices, although it is far from clear that the same outcome will occur in disks. Finally, we note that a residual amount of vorticity can be generated from finite-amplitude compressive perturbations. We have performed a series of runs with zero initial vorticity and perturbation wavelengths on the order of the scale height, and the results are qualitatively similar to Figure 5 with the shear stress reduced by nearly two orders of magnitude.

This work was supported by NSF grant AST 00-03091 and PHY 02-05155, and a Drick-amer Fellowship for BMJ.

REFERENCES

Balbus, S. A. 2000, *ApJ*, 534, 420

Balbus, S. A. 2003, *ARA&A*, 41, 555

Balbus, S. A. & Hawley, J. F. 1991, *ApJ*, 376, 214

Balbus, S. A., Hawley, J. F., & Stone, J. M. 1996, *ApJ*, 467, 76

Balbus, S. A., & Hawley, J. F. 1998, *Reviews of Modern Physics*, 70, 1

Baptista, R., Horne, K., Wade, R. A., Hubeny, I., Long, K. S., & Rutten, R. G. M. 1998, *MNRAS*, 298, 1079

Baptista, R. 2004, *Astronomische Nachrichten*, 325, 181

Barge, P., & Sommeria, J. 1995, *A&A*, 295, L1

Barranco, J. A., & Marcus, P. S. 2005, ArXiv Astrophysics e-prints, astro-ph/0501267

Blaes, O. M., & Hawley, J. F. 1988, *ApJ*, 326, 277

Desch, S. J. 2004, *ApJ*, 608, 509

Fleming, T., & Stone, J. M. 2003, *ApJ*, 585, 908

Fromang, S., Terquem, C., & Balbus, S. A. 2002, *MNRAS*, 329, 18

Gammie, C. F. & Menou, K. 1998, *ApJ*, 492, L75

Gammie, C. F. 2001, *ApJ*, 553, 174

Godon, P., & Livio, M. 1999, *ApJ*, 523, 350

Godon, P., & Livio, M. 2000, *ApJ*, 537, 396

Gough, D. O. 1969, *Journal of Atmospheric Sciences*, 26, 448

Hawley, J. F. 1987, *MNRAS*, 225, 677

Hawley, J. F. 1990, *ApJ*, 356, 580

Hawley, J. F., Gammie, C. F., & Balbus, S. A. 1995, *ApJ*, 440, 742

Johnson, B. M. & Gammie, C. F. 2005, *ApJ*, submitted

Kerswell, R. R. 2002, Annual Review of Fluid Mechanics, 34, 83

Klahr, H. H. & Bodenheimer, P. 2003, ApJ, 582, 869

Knobloch, E., & Spruit, H. C. 1986, A&A, 166, 359

Kunz, M. W. & Balbus, S. A. 2004, MNRAS, 348, 355

Li, H., Finn, J. M., Lovelace, R. V. E., & Colgate, S. A. 2000, ApJ, 533, 1023

Li, H., Colgate, S. A., Wendorff, B., & Liska, R. 2001, ApJ, 551, 874

Lovelace, R. V. E., Li, H., Colgate, S. A., & Nelson, A. F. 1999, ApJ, 513, 805

Masset, F. 2000, A&AS, 141, 165

Menou, K. 2000, Science, 288, 2022

Menou, K., & Quataert, E. 2001, ApJ, 552, 204

Narayan, R., Goldreich, P., & Goodman, J. 1987, MNRAS, 228, 1

Papaloizou, J. C. B., & Pringle, J. E. 1984, MNRAS, 208, 721

Papaloizou, J. C. B., & Pringle, J. E. 1985, MNRAS, 213, 799

Press, W. H. 1978, Comments on Astrophysics, 7, 103

Sano, T., & Stone, J. M. 2003, ApJ, 586, 1297

Stone, J. M., Gammie, C. F., Balbus, S. A., & Hawley, J. F. 2000, Protostars and Planets IV, 589

Stone, J. M. & Norman, M. L. 1992, ApJS, 80, 753

Umurhan, O. M. & Regev, O. 2004, A&A, 427, 855

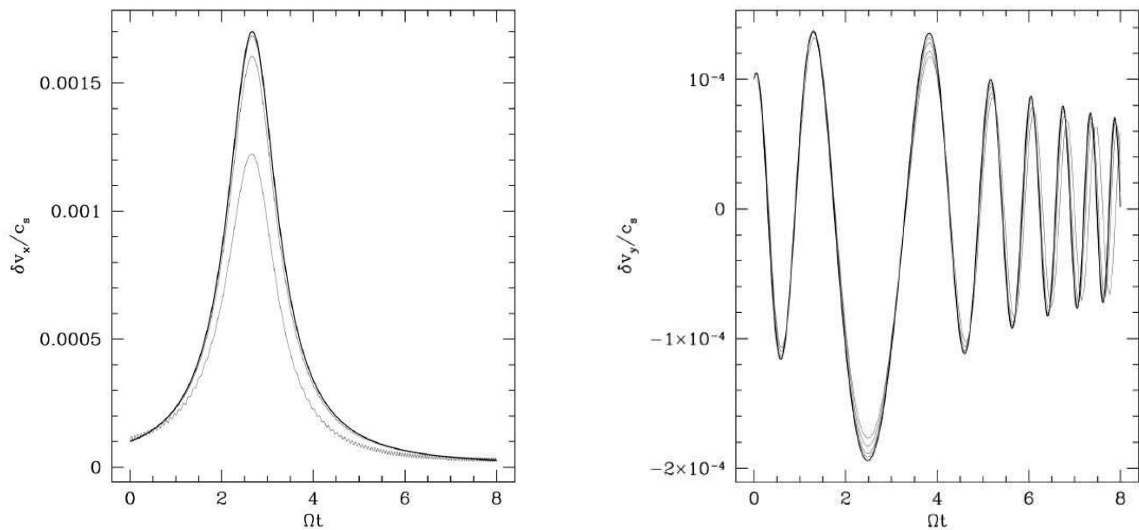


Fig. 1.— Evolution of velocity amplitudes for a vortical (left) and non-vortical (right) shwave. The heavy line is the analytic result, and the light lines are numerical results with (in order of increasing accuracy) $N_x = N_y = 32, 64, 128$ and 256.

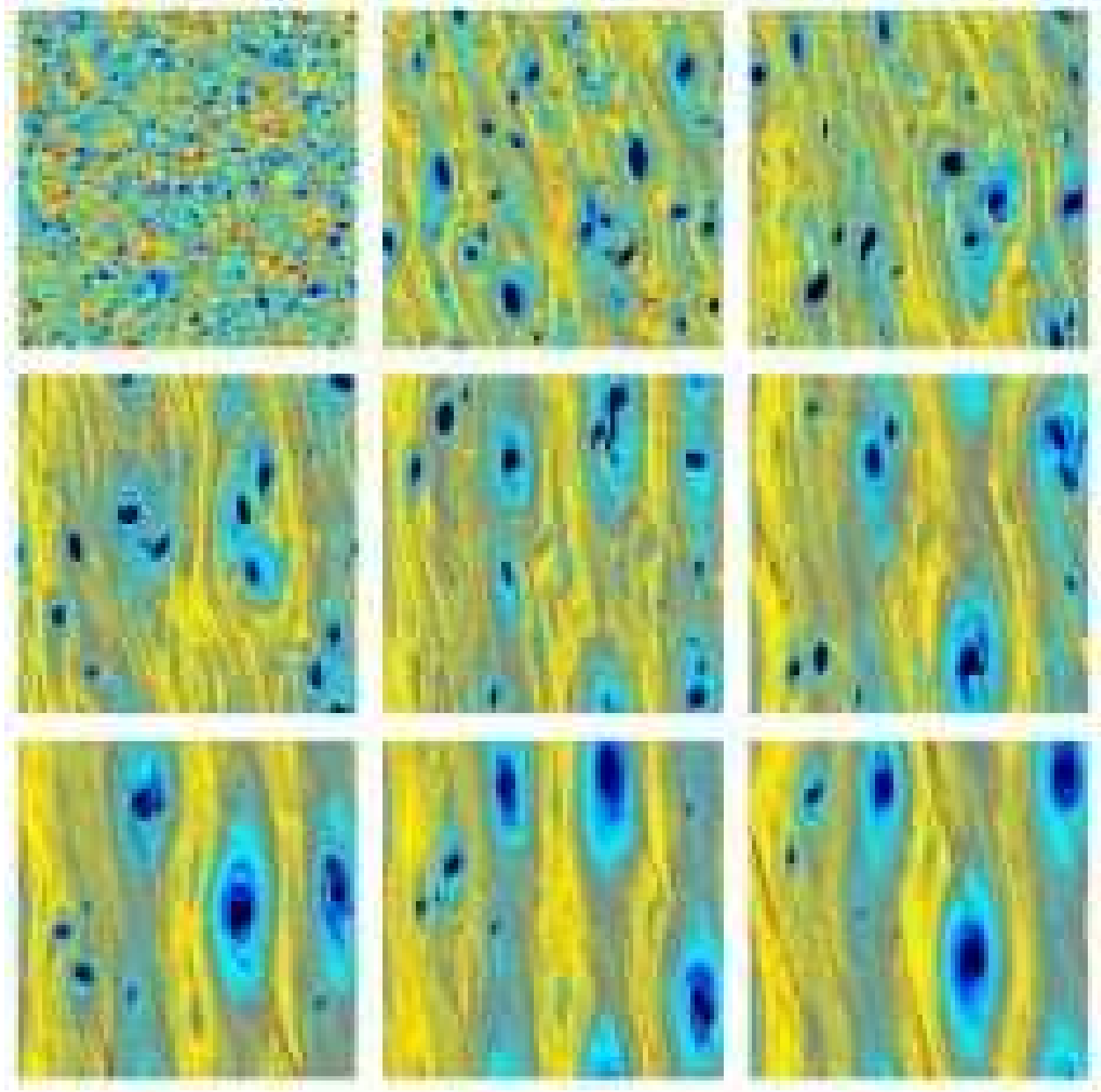


Fig. 2.— Panels show the evolution of the potential vorticity in the fiducial run. The size is $4H \times 4H$ and the numerical resolution is 1024^2 . The initial conditions are shown in the upper left corner, and the other frames follow in lexicographic order at intervals of $22.2\Omega^{-1}$. Dark shades (blue and black in electronic edition) indicate potential vorticity smaller than $\Omega/(2\Sigma_0)$; light shades (yellow and red in electronic edition) indicate positive potential vorticity perturbations. Evidently only the “anticyclonic” (negative potential vorticity perturbation) vortices survive. Each vortex sheds sound waves, which steepen into trailing shocks.

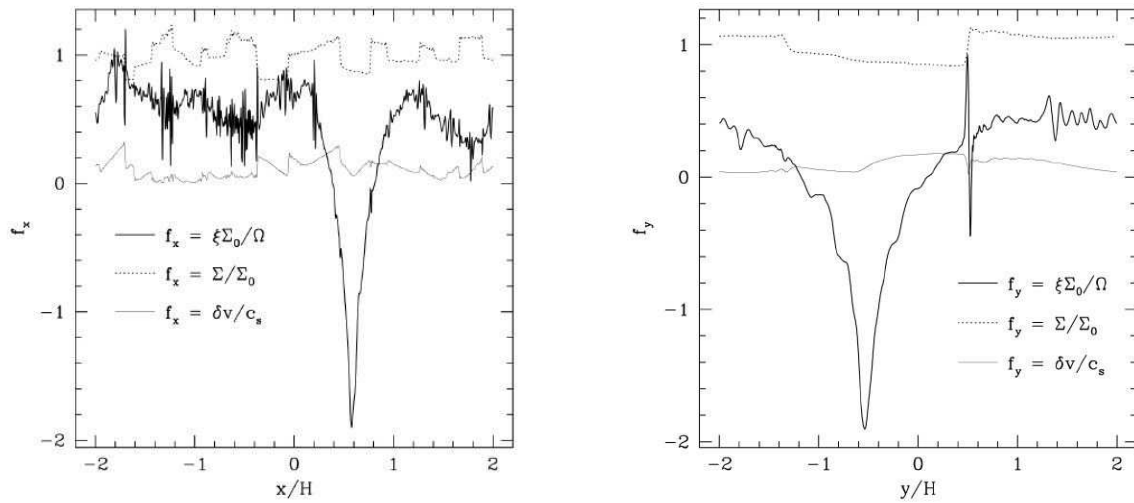


Fig. 3.— Radial (left) and azimuthal (right) slice of a vortex at the end of the fiducial run. The heavy line shows the potential vorticity, the light line shows the magnitude of the velocity and the dotted line shows the surface density.

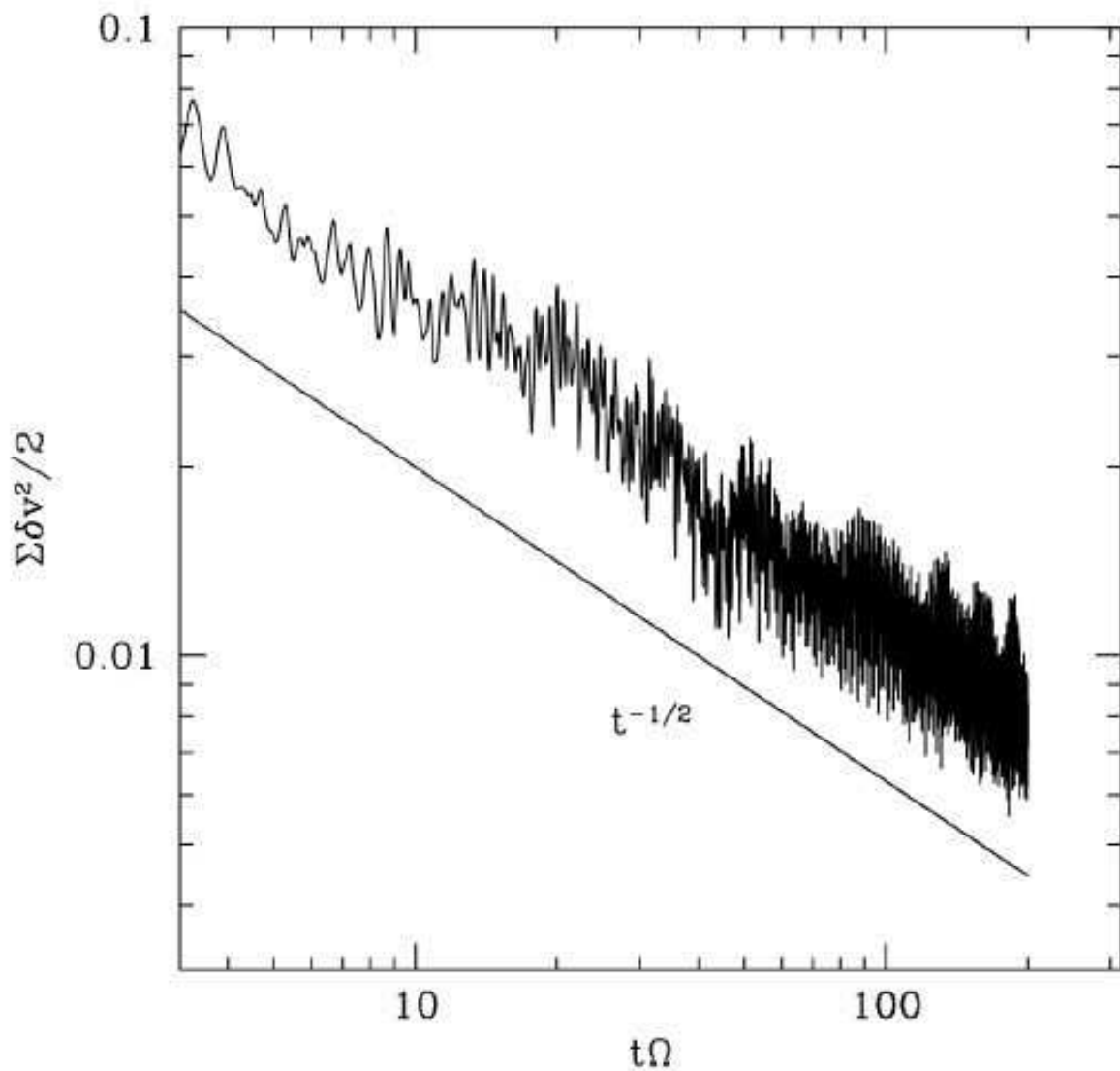


Fig. 4.— Evolution of kinetic energy in time for the fiducial run, on a log-log scale. The solid line shows a $t^{-1/2}$ decay for comparison purposes.

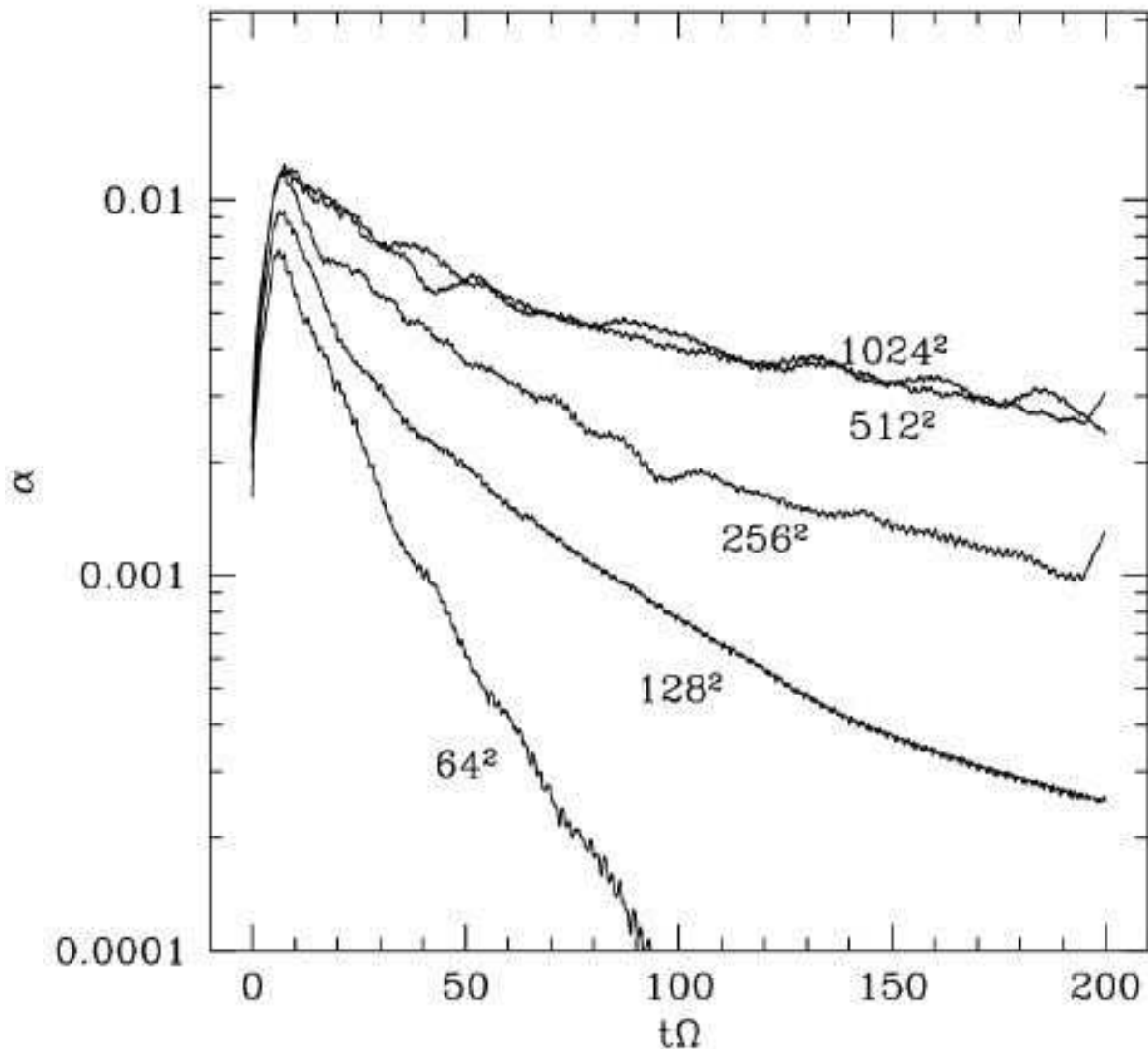


Fig. 5.— Evolution of the shear stress α in the fiducial run and a set of runs at lower resolutions.

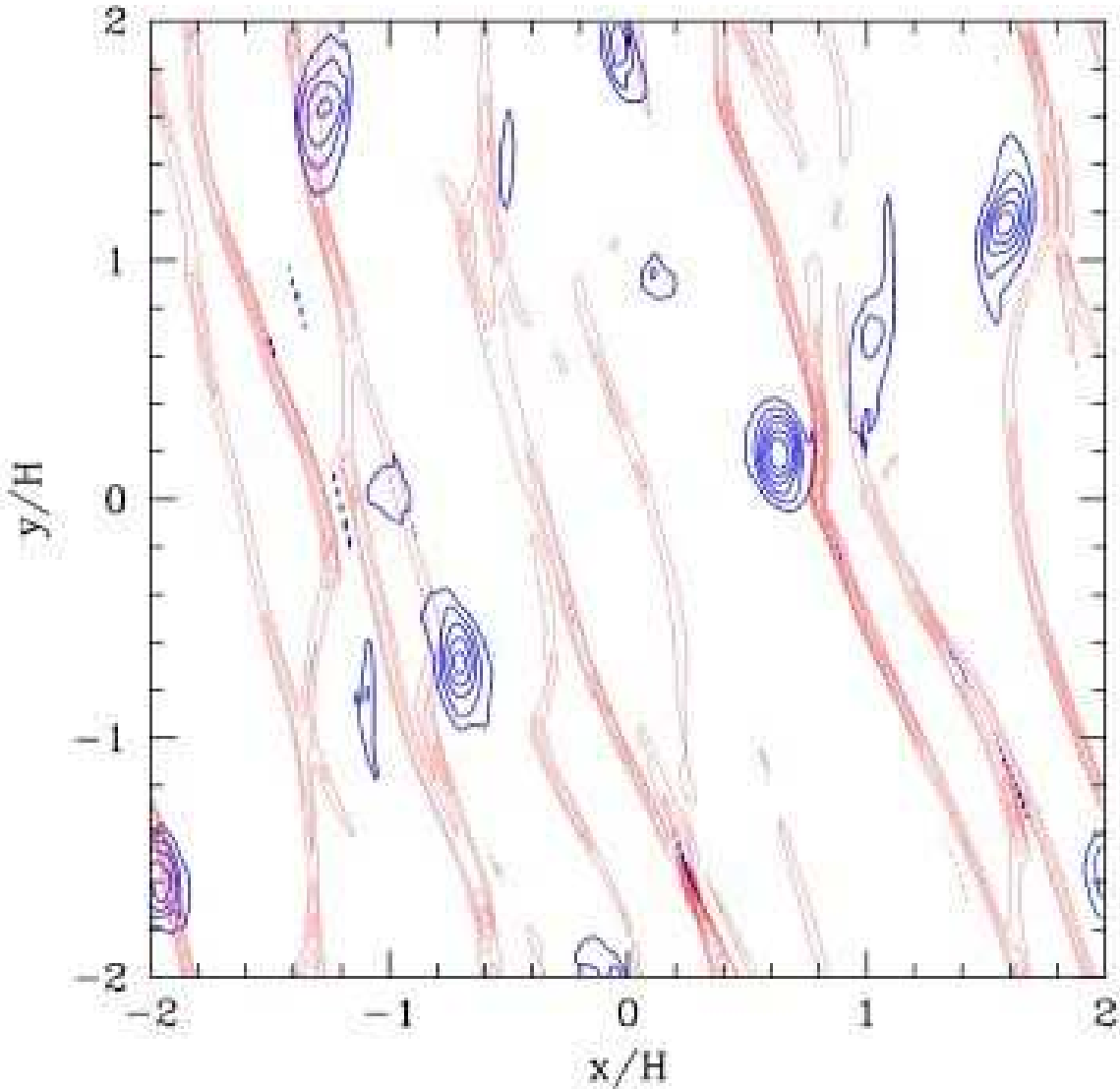


Fig. 6.— Snapshot of the velocity divergence superimposed on the potential vorticity in a medium-resolution (256^2) version of the fiducial run. The thin (red in electronic edition) contours indicate negative divergence and are associated with shocks. The thick (blue in electronic edition) contours indicate negative potential vorticity.

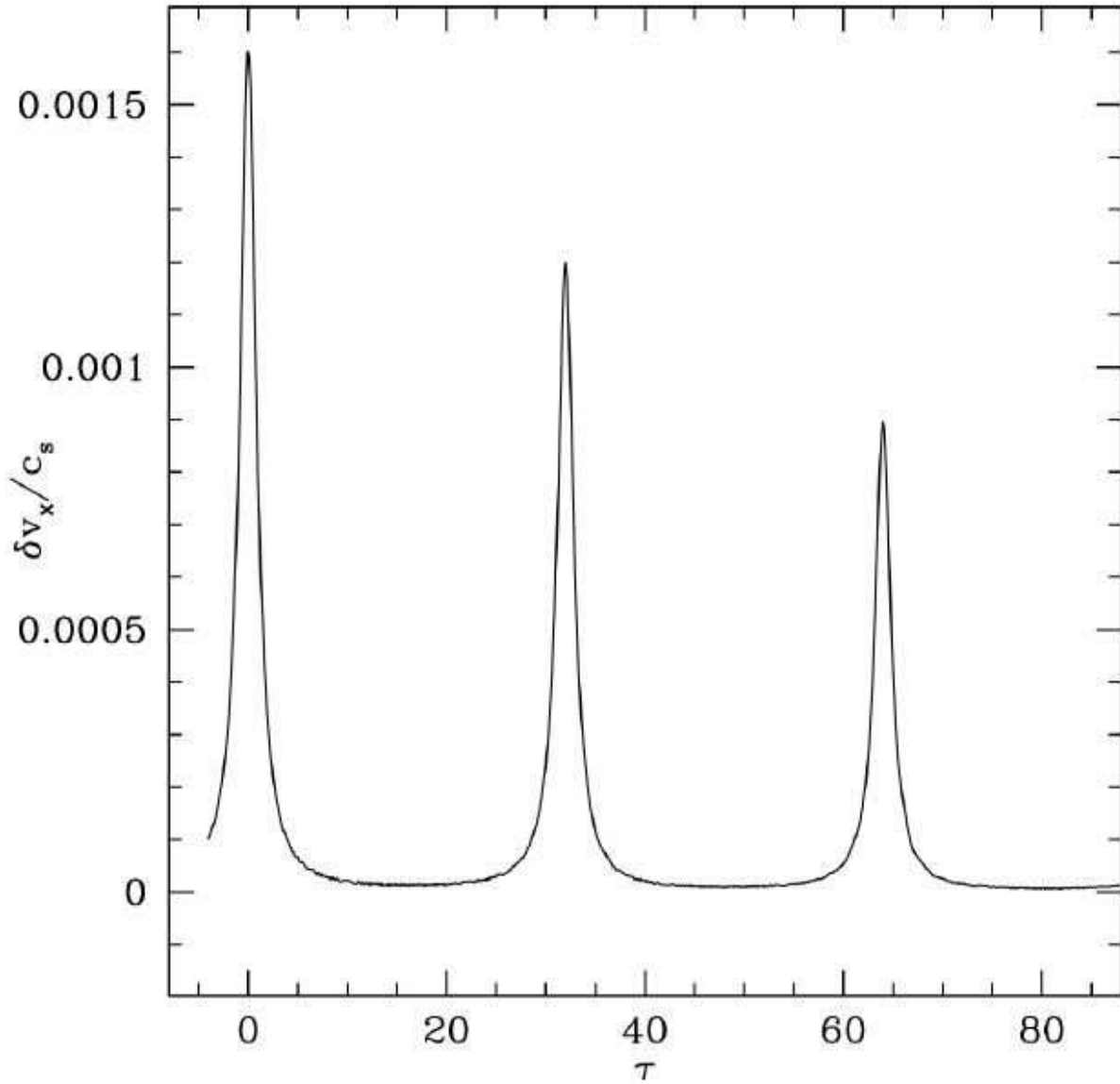


Fig. 7.— Evolution of a vortical shwave amplitude in a low-resolution (64^2) run, in units of τ . The initial shwave vector (k_{x0}, k_y) is $(-16\pi/L_x, 4\pi/L_y)$, corresponding to $\tau_0 = -4$. The interval between successive peaks (a numerical effect due to aliasing) is $\tau = N_x/n_y$, where $n_y = 2$ is the azimuthal wavenumber.

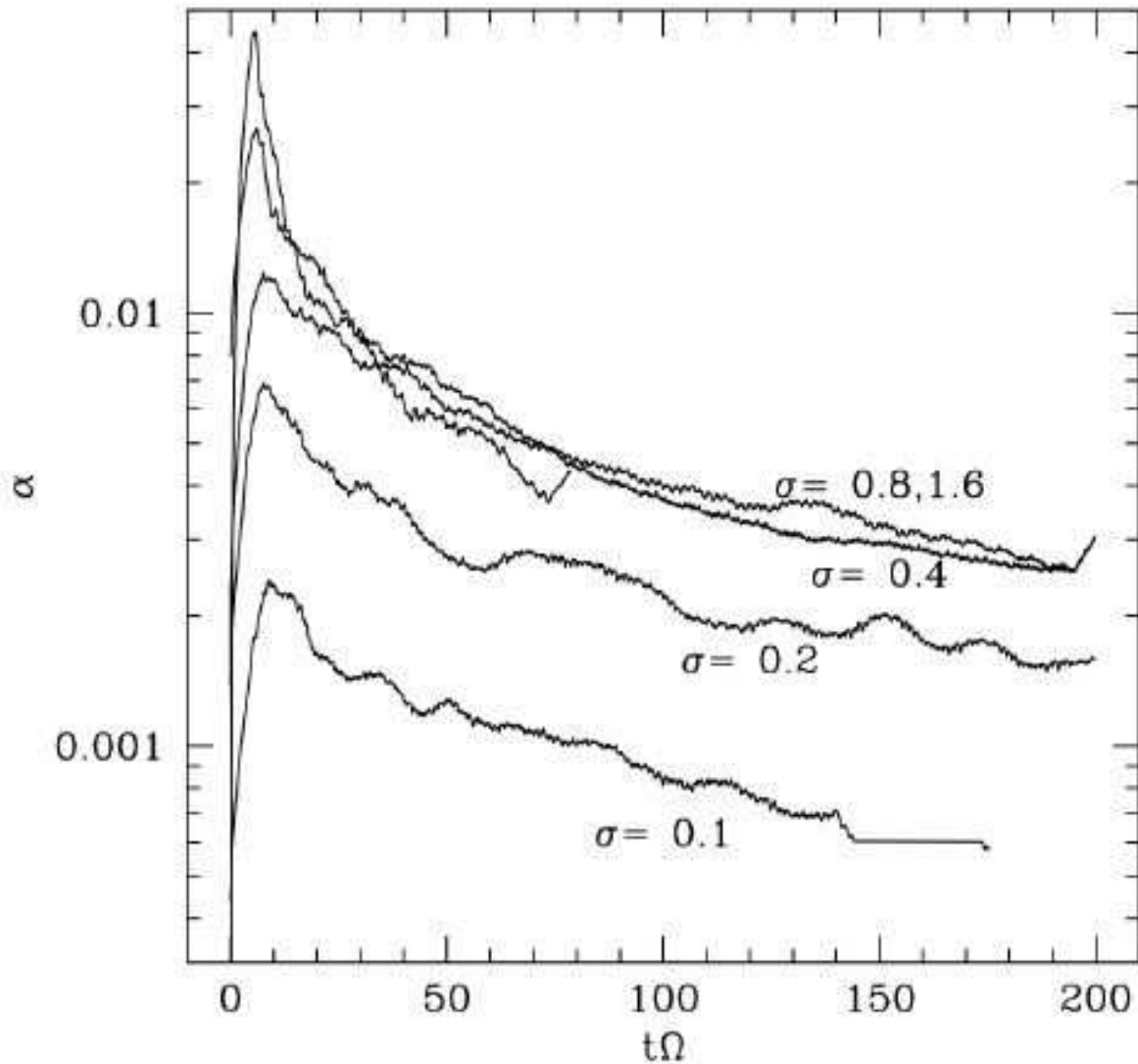


Fig. 8.— Evolution of the shear stress α in a set of runs with varying initial σ . Apparently for low values of σ the shear stress is reduced, but for initial Mach number near 1 the stress saturates. All runs have $L = 4H$.

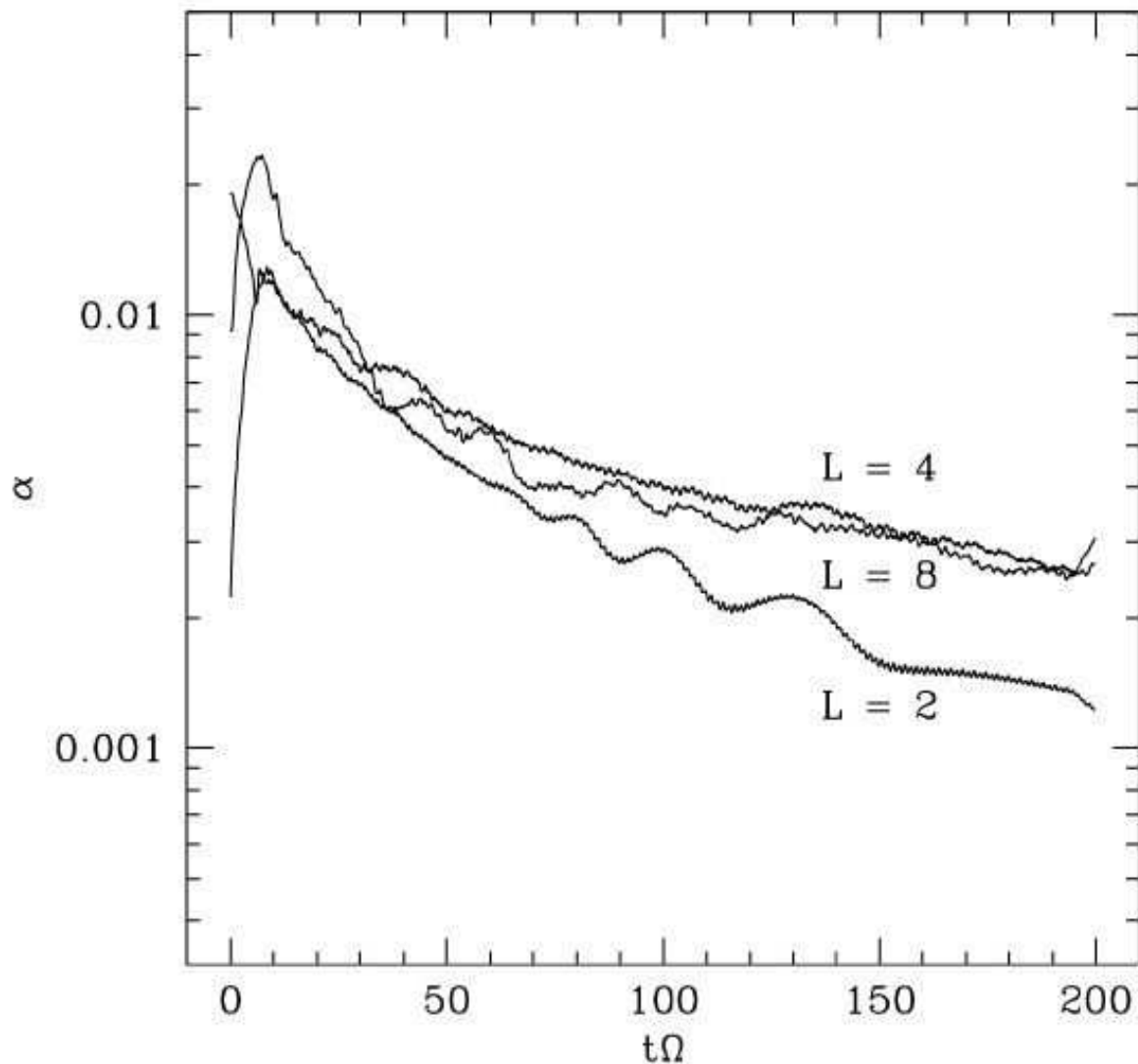


Fig. 9.— Evolution of the shear stress α in a set of runs at with varying initial L , but the same initial Mach number σ .

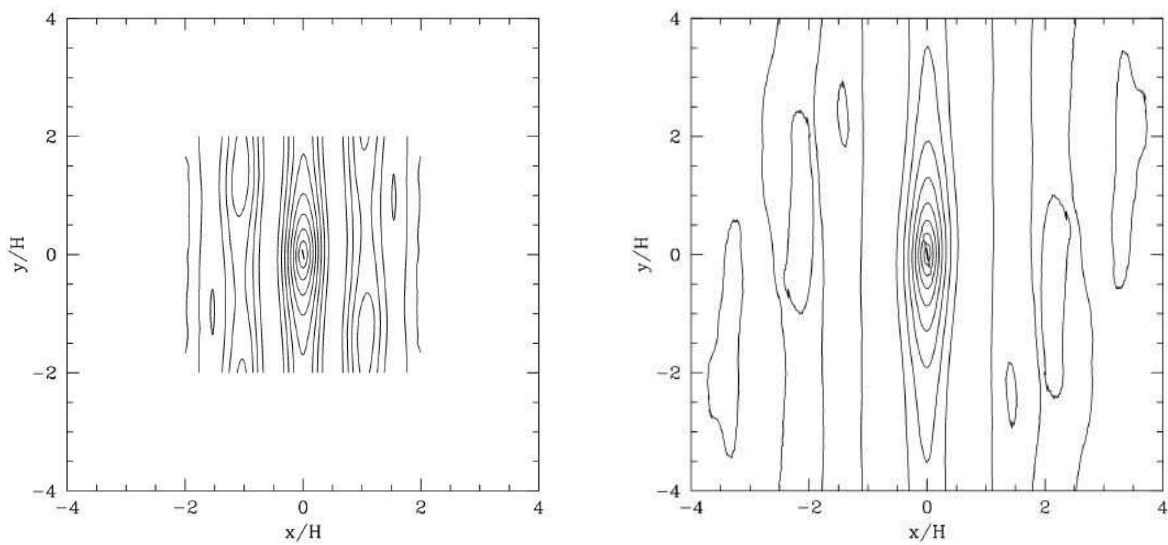


Fig. 10.— Autocorrelation function of the potential vorticity ξ for the fiducial model with $L = 4H$ (left) and a model with $L = 8H$ (right).